Optical absorption and transport in semiconducting $SrTiO_3$†

C. Lee, J. Destry*, and J. L. Brebner
Département de Physique, Université de Montréal, Montréal, Québec, Canada
(Received 13 June 1974)

The optical absorption of reduced and doped $SrTiO_3$ has been measured between 0.39 and 7 μm. Transport measurements were also carried out between room temperature and 10 K for various samples with different treatment. Both optical and transport properties were found to depend greatly on the methods of preparations of the samples. We found up to five absorption peaks in the visible and infrared regions, lying at 0.43, 0.52, 0.70, 1.2, and $\sim$ 4.8 μm. In all samples, the so called free-carrier absorption tail starts falling off at about 2.5 μm and has a maximum between 4.5 and 5 μm. The position of this peak cannot be explained by the free-carrier absorption theory of LO-mode scattering. The new absorption mechanisms are introduced in order to explain the results in this wavelength region. Of the five absorption peaks, the first, second, and fourth peaks are due to impurity or defect levels, whereas the third and fifth peaks are interpreted as being due either to interconduction-band or vacancy-level to conduction-band transitions. The conduction and scattering mechanisms are discussed.

I. INTRODUCTION

Stimulated by the transport measurements of Frederikse *et al.*[1] and by the energy-band calculation of Kahn and Leyendecker,[2] considerable effort has been directed toward the understanding of electronic scattering and conduction mechanisms in semiconducting strontium titanate by many workers[3–7] in the past decade. These efforts were backed up by optical absorption measurements[8–11] and further energy-band calculations.[12–14] It is now accepted that the transport mechanism in doped and heavily reduced samples at moderate to high temperatures is due to the motion of conduction electrons scattered by longitudinal-optical (LO) phonons.[3–5] On the other hand, in slightly reduced samples, an additional transport mechanism at low temperatures, impurity-band-type conduction, is found.[5]

In order to study the conduction and scattering mechanisms in reduced $SrTiO_3$, Baer[9] measured the optical absorption in the visible and near-infrared regions. He observed that the absorption coefficient followed a power law as a function of wavelength with an exponent of 2.5 in the wavelength region between 0.6 and 2 μm. He concluded that the absorption was due to free carriers scattered by LO phonons, as predicted by theoretical calculations.[15,16] However, his experimental values of the absorption coefficient were an order of magnitude larger than the theoretical ones. Yamada and Miller,[10] on the other hand, observed three prominent absorption peaks extending to 1 μm. The so-called "free-carrier absorption tail" followed a power law with exponent 2.2 or less. Earlier, Gandy's data[8] had shown another peak at 1.2 μm and all results prior to this had shown that the "free-carrier absorption tail" does not strictly follow a power law but starts falling off at longer wavelengths. Measurements were not extended to long enough wavelengths for a systematic study of this deviation.

The observed values of mobility at low temperatures are orders of magnitude smaller[3] than those calculated assuming ionized impurity scattering.[17] Recently several attempts were made to determine gap level assignments using thermochromism[11,18,19] and thermally stimulated current measurements[20] for pure and transition-metal-doped crystals. Results of energy-band calculations[2,12] conflict with one another as to the location of the conduction-band minima. Even though several attempts[21,22] were made to clarify this point it is still not established one way or the other.

In view of these several facts, we have made an extensive study of this material using a variety of samples treated in different ways. The carriers were introduced by reduction, doping, and irradiation. Samples underwent different heat treatment. We have extended optical absorption measurements up to 7 μm and studied the effect of heat treatment on the transport and optical properties. Using our data, we have attempted to explain the transport and absorption mechanisms in a consistent way, taking into account existing theoretical and experimental work.

II. SAMPLE PREPARATION AND EXPERIMENTAL PROCEDURE

Pure and Nb-doped single crystals of $SrTiO_3$ were obtained from N. L. Industries (formerly National Lead Co.). The crystal boules were annealed in air at 1400 °C for 48 h, by N. L. Industries before shipping. A diamond saw was used to cut the boules into wafers of the desired thicknesses (0.2 ~ 3 mm), and these were then polished with a slurry of Linde

TABLE I. Sample-preparation data.

Sample no.	Reduction Temp. (°C)	Reduction Time (hr: min)	Atmosphere	Doping and other treatment	Abs. coef. at 1.5 μm (cm^{-1})	Carrier conc. at 300 K (cm^{-3})
RST1	1350	2:00	vac	9-MeV proton irradiation, 1 $\mu A/cm^2$	96[a]	
ST22	1000	2:00	vac	···	113.0	
ST23	800	1:40	vac	···	16.5	5×10^{17}
ST25	850	1:35	vac	···	65.8	
ST27	750	1:35	vac	···	6.92	1.22×10^{17}
ST30	750	2:00	H_2	1700 °C, 1 hr preannealing in air	37.1	1.53×10^{18}
ST31	1000	2:00	H_2	···	105.2	
ST32	900	2:00	H_2	···	50.9	
ST34	752	2:35	H_2	···	19.0	
ST39	750	2:00	H_2	···	22.0	4.24×10^{17}
ST47	709	1:55	H_2	···	36.9	
ST48	663	1:50	H_2	···	11.1	1.00×10^{17}
ST49	658	1:51	H_2	···	10.0	
ST52	658	1:51	H_2	Nb: 3×10^{18} cm^{-3}	10.8	6.21×10^{17}
ST53	711	1:55	H_2	Nb: 3×10^{18} cm^{-3}	15.4	
ST54	757	1:47	H_2	Nb: 3×10^{18} cm^{-3}	91[a]	6.0×10^{18}
ST55	805	1:55	H_2	Nb: 3×10^{18} cm^{-3}	26.5	
ST56	654	1:53	H_2	Nb: 3×10^{18} cm^{-3}	4.84	
ST61	···	···	···	Nb: 0.03 wt%	···	1.55×10^{18}
ST62	···	···	···	Nb: 0.03 wt%	31.3	1.55×10^{18}
ST63	···	···	···	Nb: 0.03 wt%	31.7	1.55×10^{18}
ST64	805	1:54	H_2	Nb: 0.03 wt%	132[a]	
ST65	705	1:47	H_2	Nb: 0.03 wt%	29.3	1.55×10^{18}
ST71	900	1:55	H_2	Nb: 0.05 wt% 1000 °C, 4 hrs. in vac.	230[a]	
ST72	···	···	···	Nb: 0.05 wt% 1000 °C, 4 hrs. in vac.	55[a]	3.34×10^{18}
ST73	···	···	···	Nb: 0.05 wt% 1000 °C, 4 hrs. in vac.	46.3	3.34×10^{18}

[a]Extrapolated value.

A, B, and C polishing powder. Final cutting of the polished wafers into rectangular shapes (typically $4\times12\ mm^2$) was effected with a string saw. Preannealing to reduce the dislocation density on one sample was carried out by heating it (after it had already been cut and polished) in air at 1700 °C for 1 h and then by cooling it down to room temperature very slowly in a gas-fired corundum furnace. Nb doping was effected during crystal growth by adding predetermined amounts of niobium oxide into the feed material. Reduction was carried out either in a hydrogen atmosphere or in the hard-vacuum furnace, after prebaking the whole system. Proton irradiation was performed on a thin sample using the 10-MeV Van de Graaff of the University of Montreal. Methods of reduction and doping as well as of heat treatment are given in Table I.

Optical absorption measurements were carried out by employing both double-beam and single-beam sample-in–sample-out methods using a Jarrell-Ash model 78-466 scanning spectrometer, a Cary model 17 spectrophotometer, and a Perkin-Elmer infrared spectrophotometer.

A standard dc four-probe method was employed to measure the electrical resistivity and Hall coefficient using a Dana model 5800, six-digit digital voltmeter coupled with an Anadex model DP-650 digital printer. Current and potential contacts were made using pure-indium solder with an ultrasonic soldering gun. Indium made much better and stronger contacts with polished surfaces than with unpolished ones. Samples were mounted on a variable-temperature insert of the Minnesota Valley engineering model HLDT3 cryostat. Temperature of the sample was monitored by two sets of copper-constantan thermocouples with test junctions

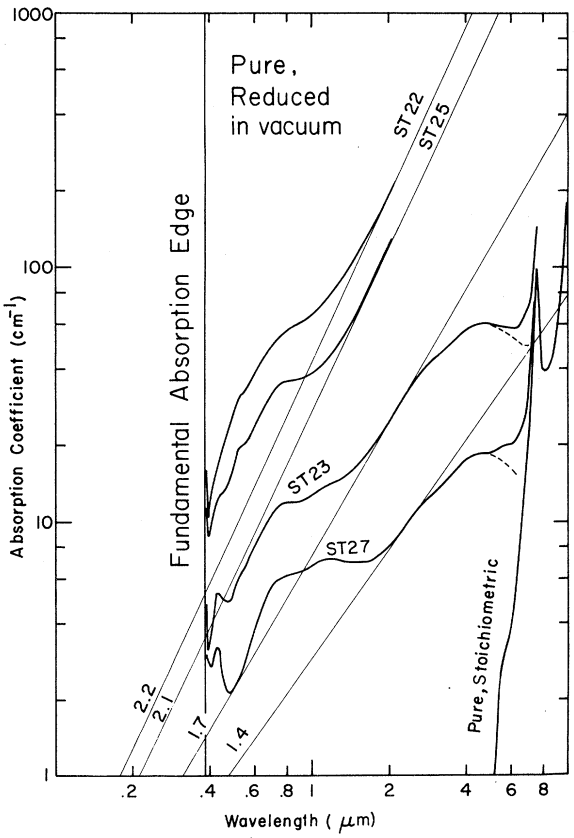

FIG. 1. Log-log plot of the absorption coefficient vs wavelength for undoped and unannealed samples reduced in vacuum. The absorption curve for the pure, stoichoimetric crystal is also included. Numbers on the straight-line tangents to the steepest portion of the infrared tail represent the slopes of that portion. Dotted por- above 5μ m for ST23 and ST27 represents net absorption after subtracting the infrared absorption of the stoichiometric samples.

on a dummy sample and the reference junctions at the ice point or at liquid-helium temperature. The typical magnetic field used for Hall measurements was 6.6 KG and supplied by a Magnion L-75B electromagnet.

III. EXPERIMENTAL RESULTS

A. Optical absorption

The log-log plots of the absorption coefficient against wavelength are shown in Fig. 1 for pure samples reduced in vacuum and in Fig. 2 for the pure samples reduced in a hydrogen atmosphere. Also included in Fig. 2 are the absorption curves for the sample (ST30) which underwent high-temperature preannealing prior to the reduction and for the sample irradiated with 9-MeV protons in a vacuum chamber. (For detailed reduction processes refer to the Table I.)

The absorption curves for the reduced samples show essentially the same characteristics whether they are reduced in vacuum, in a hydrogen atmosphere, or by proton irradiation. Altogether there are five absorption peaks in the wavelength range between 0.4 and 7 μm: These are at 0.43 μm (2.9 eV), 0.52 μm (2.4 eV), 0.7 μm (1.7 eV), 1.2 μm (1 eV), and somewhere between 4.5 and 5 μm (0.25~0.28 eV), which we designate as peaks No. 1, 2, 3, 4, and 5, respectively. The first three peaks in the visible region have also been seen by other workers[9-11] at one time or another. The fourth peak, at 1.2 μm, was observed by Gandy[8] and can be more easily seen for the low-reduction samples. Note that it is missing for the crystal annealed at 1700 °C (ST30). The peak No. 5. near 5 μm had not been observed because no measurements of absorption in this wavelength range had been made to date. Barker's reflectivity measurement,[23] however, indicates the existence of this peak. Baer[9] measured absorption to 4 μm for one sample and saw the initial part of the fifth peak.

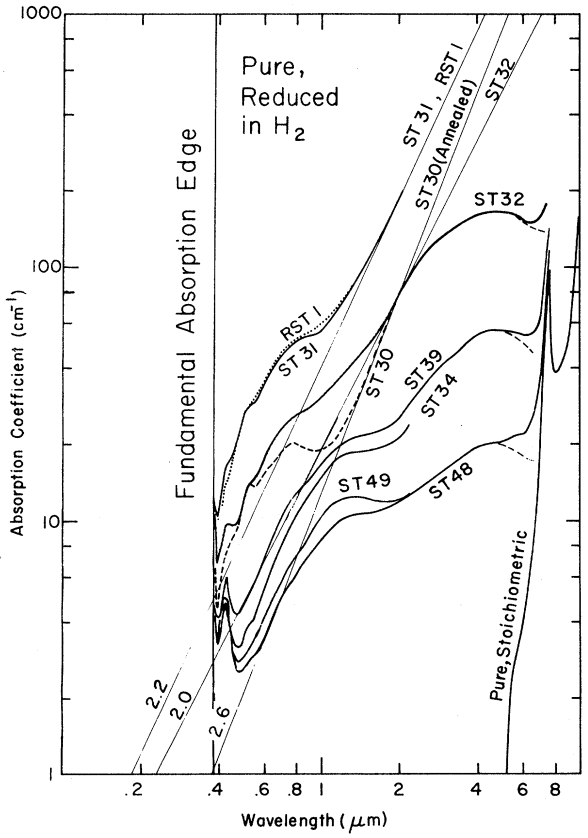

FIG. 2. Log-log plot of the absorption coefficient vs wavelength for the undoped samples reduced in hydrogen atmosphere. ST30 (dotted curve) is preannealed at 1700 °C prior to reduction and RST1 is irradiated with 9-MeV protons in vacuum.

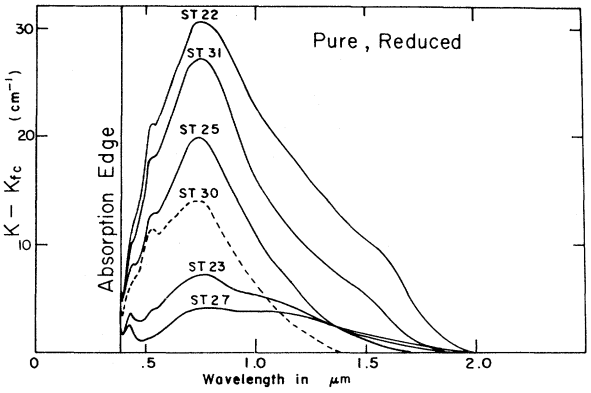

FIG. 3. Absorption coefficient minus the tangent to the steepest portion in the infrared plotted against the wavelength in linear scale. The dotted curve is for the pre-annealed sample (ST30).

According to theory, free-carrier absorption is proportional to λ^n, with $n = 1.5 \sim 2.0$ for acoustic-phonon scattering,[24,25] 2.5 for longitudinal-optical-phonon scattering,[15,16] and 3.0 for ionized impurity scattering.[26–28] In the case of an absorption due to electronic transitions from a hydrogenic localized state to a higher continuum state, $n = 3.5$.[28] The slope of the straight-line portion on a log-log plot of wavelength versus absorption could, in principle, give the nature of the free-carrier absorption. As one notes from Figs. 1 and 2, however, there is hardly such a straight-line portion to the graph for unannealed, pure samples. On the other hand, for the high-temperature annealed sample, as well as for the niobium-doped samples, a straight-line portion of considerable length exists between the No. 3 and 5 peaks. This segment of the absorption curve is usually interpreted[9,10] as being due to a free-carrier absorption process, but, as we show later, we believe it to be due to another mechanism. To offset the influence of the No. 5 peak, we have subtracted what might be termed a "free-carrier tail"—the tangent to the steepest portion of the curve—from the total absorption and the result is shown in Fig. 3. We will continue to use the term "free-carrier tail" for this portion of the absorption curve in order to make comparison with previous work easier. The size of the third peak at 0.7 μm increases rapidly as the degree of reduction is increased, while the first two peaks seem to saturate quickly.

In Fig. 4, the absorption curves are given for heavily doped samples (0.03- and 0.05-wt% Nb nominal). The two bottom curves are for the Nb-doped samples without any reduction. Only the No. 2 peak at 0.52 μm in the visible region and the No. 5 peak near 5 μm can be seen and, moreover, the "free-carrier tail" has a steep slope of more than 3. The top two curves are for the samples heavily doped with Nb and then reduced in a hydrogen atmosphere. The enhancement of the No. 3 peak at 0.7 μm by the reduction process is evident, while the No. 2 peaks remain essentially unchanged.

In Fig. 5 we show the absorption curves for the samples slightly doped with Nb (3×10^{18} cm^{-3} nominal) and then reduced in a hydrogen atmosphere at various temperatures. Prior to reduction, these samples are clear, colorless insulators like the pure crystal. After reduction one observes peaks No. 1–3 in the visible, and No. 5 near 5 μm in the infrared will be seen later in Fig. 9. As before, the No. 3 peak is enhanced by the reduction, whereas the Nos. 1 and 2 peaks are more or less unaffected. Note that the first peak in the sample with lowest reduction (ST56) is missing. Again the "free-carrier tails" have a slope of about 3 except for the most heavily reduced sample (ST54), which has a slope of 2.5. It is evident from the results so far given that, by Nb doping, the slope of the so called "free-carrier tail" is increased while the size of the No. 4 peak is decreased. The first three absorption peaks in the visible region are compared in Fig. 6 for the representative samples

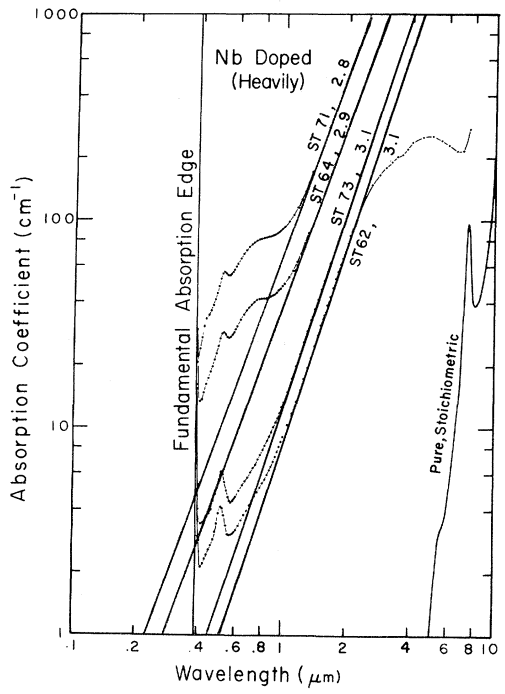

FIG. 4. Log-log plot of the absorption coefficient vs wavelength for samples doped heavily with Nb. ST62 and ST73 are doped with 0.03 and 0.05-wt% Nb, respectively, without any reduction, whereas ST64 and ST71 are doped (0.03- and 0.05-wt% Nb) and then reduced in hydrogen atmosphere at 800 and 900° C, respectively.

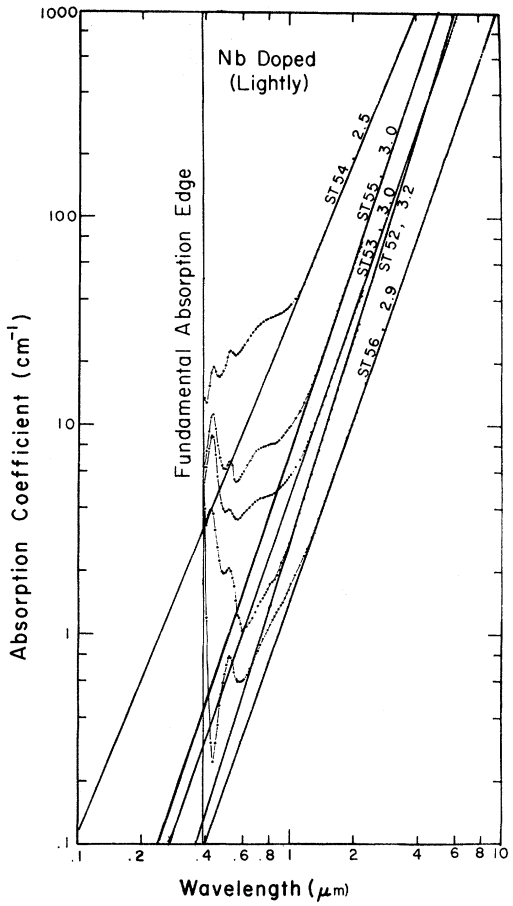

FIG. 5. Log-log plot of the absorption coefficient vs wavelength for the lightly Nb-doped (3×10^{18} cm^{-3}) samples after reduction.

with different kinds of reducing and doping treatments. When the reduced sample is oxidized or annealed in air at successively higher temperatures, a whole set of absorption curves similar to the one for the reduced samples with decreasing degree of reduction is obtained, as shown in Figs. 7 and 8 for the pure, reduced sample (ST47), and in Fig. 9 for the doped, reduced sample (ST55). The size of the third peak at 0.7 μm decreases rapidly as the oxidation temperature is raised, whereas the other peaks stay more or less constant until they disappear abruptly. The absorption introduced by reduction disappears completely at an oxidation temperature lower than the reduction temperature at which they were introduced. The slope of the "free-carrier tail" of the doped plus reduced sample (ST55) remains unchanged by the oxidation, and that of the pure, reduced sample (ST47), on the other hand, decreases slowly as the oxidation temperature is raised.

B. Transport

In Fig. 10 the electrical resistivity is plotted against reciprocal temperature on a log-log scale. For the pure, reduced samples (ST27, ST39, and ST48) as the temperature is lowered, the resistivity increases at first, reaches a maximum, and then decreases to a constant value, confirming our previous result.[5] On the other hand, for the doped, doped and reduced, and preannealed and reduced samples (ST61, ST54, and ST30, respectively), the resistivity decreases monotonically as temperature is lowered, agreeing with the results of Frederikse *et al.*[4] and Tufte *et al.*[3]

A marked difference is also seen in Hall coefficient between these two sets of crystals as shown in Fig. 11. For pure, reduced crystals (ST27, ST39, and ST48) the Hall coefficient increases rapidly and then flattens out at about 100 K and finally reaches a constant value near 25 K. There is a second small jump in Hall coefficient near 40 K as before.[3,5,7] The preannealed and doped crystals (ST30, ST54, and ST61), on the other hand, show an almost temperature-independent Hall coefficient.

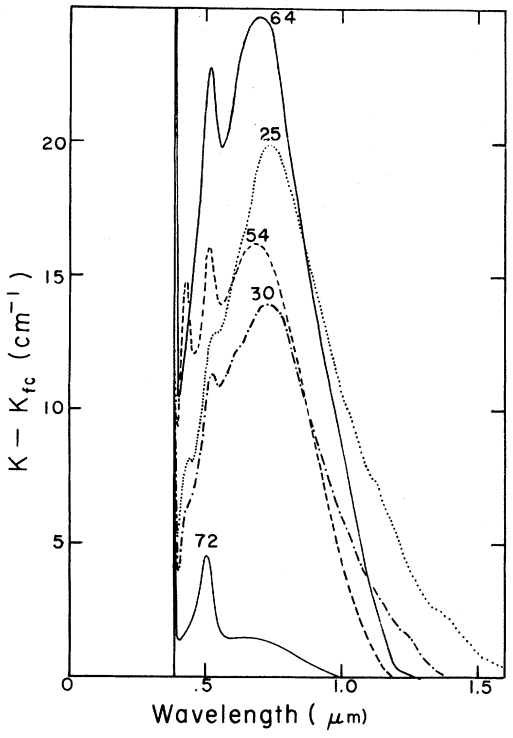

FIG. 6. Comparison of the absorption peaks for typical samples with different sample treatments. ST64: heavily Nb doped and reduced; ST25: pure, unannealed, reduced; ST54: lightly Nb doped and reduced; ST30: preannealed and reduced; ST72: heavily Nb doped.

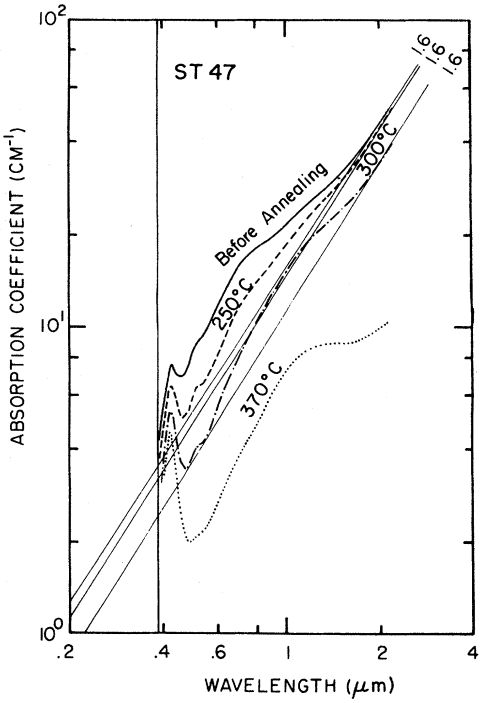

FIG. 7. Log-log plot of the absorption vs wavelength for ST47 showing the decrease in absorption by the oxidation at successively higher temperatures. ST47 was undoped, unannealed, and reduced in hydrogen atmosphere at 700 ° C.

Note that the reduced sample ST30 shows even a decrease in Hall coefficient at low temperature. Thus pure, reduced crystals, without preannealing, show a carrier freeze-out effect, implying the existence of relatively deep donor levels, [3,5] while the donor levels in the doped and preannealed samples

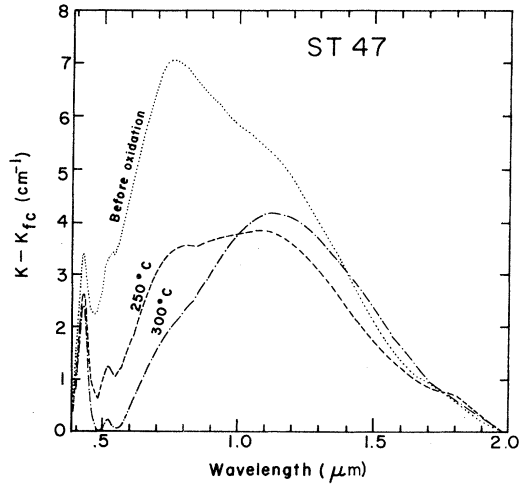

FIG. 8. Change in absorption peaks by successive oxidation for ST47.

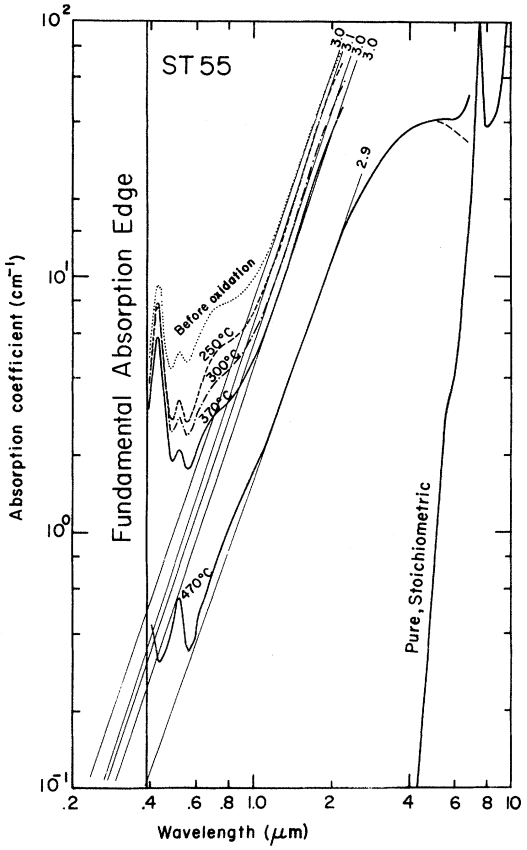

FIG. 9. Log-log plot of the absorption vs wavelength for ST55 showing the decrease in absorption by oxidation at successively higher temperatures. ST55 was initially doped with 3×10^{-18} - cm^{-3} Nb and then reduced at 800 °C.

are very shallow and very close to the bottom of the conduction band.

In Fig. 12 the Hall mobility is plotted against inverse temperature on a log-log scale. Again the difference between the differently treated crystals is evident: The reduced samples have low mobility at low temperature with nearly equal values while the mobility values of the doped or preannealed samples are much higher and differ from each other considerably, depending on the carrier concentration and methods of doping. The optical absorption data, as well as the transport data, show that the conduction and scattering mechanism in semiconducting strontium titanate depend sensitively on the method of sample treatment. We elaborate on this point in Sec. IV.

IV. DISCUSSION

A. Absorption peaks

In Figs. 1–9 we have seen at least 5 absorption peaks throughout the region 0.4 ~ 7 μm in pure and Nb-doped $SrTiO_3$. These fall into two categories:

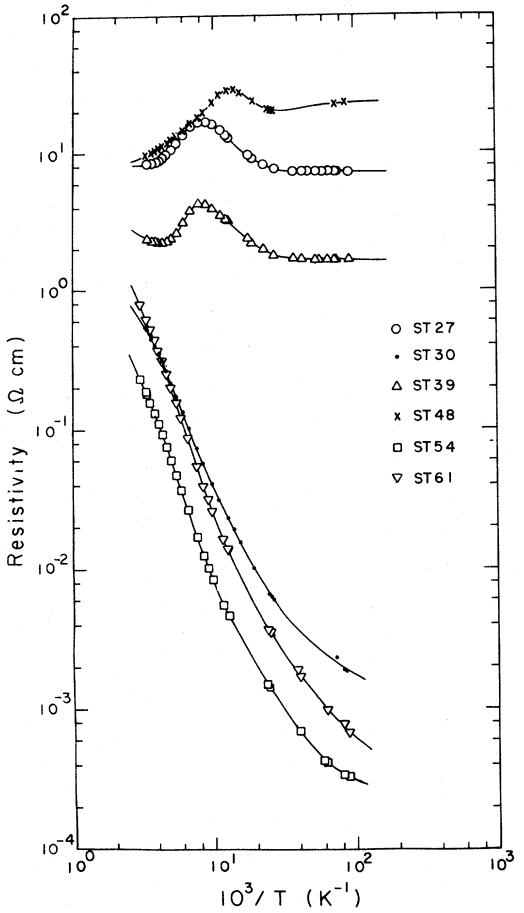

FIG. 10. Resistivity vs reciprocal-temperature curves in log-log scale for various samples. ST27 is undoped, unannealed, and reduced in vacuum at 750 °C. ST39 and ST48 are undoped, unannealed, and reduced in hydrogen atmosphere at 750 and 660 °C, respectively. ST30 is undoped, preannealed, and reduced in hydrogen at 750 °C. ST61 is heavily doped (0.03-wt% Nb) and ST54 is lightly doped (3×10^{18} Nb) and then reduced at 750 °C.

In one, the size of the peak grows indefinitely by reduction, and in the other, the size of the peak is easily saturable by reduction. We call the former a nonsaturable peak and the latter a saturable peak. Peaks No. 3 and 5 are nonsaturable, the rest are saturable. We discuss each peak separately in what follows.

Peak No. 1 at 0.43 μm (2.9 eV) is fairly narrow and can be found in most samples. It is missing, however, in Nb-doped samples (Fig. 4), and the degree of reduction is irrelevant to the size of the peak (Fig. 6). For a given crystal it reaches a certain height with moderate reduction and then remains constant with further reduction (Fig. 5). This process is reversible as one can see in Figs. 7–9: When one tries to remove this peak by oxidation at an elevated temperature its size remains constant until it suddenly disappears at a certain critical temperature. Wild *et al.*[11] saw a strong enhancement of this peak by Fe doping, while Baer[9] did not see this peak at all, as is the case in our Nb-doped samples (Fig. 4). These facts are strong evidence that this peak is extrinsic and caused by the Fe ion. Using the EPR results of Faughnan,[18,29] Wild *et al.*[11] identified it as being due to an absorption of electrons trapped at an Fe^{4+} ion placed in a cubic site about 0.3 eV above the valence band. On the other hand, Morin *et al.*[20] place this level well above (1.06 eV) the valence band and place an Fe^{4+} V (iron-vacancy complex) level closer to the valence band. It is not clear at this stage whether Fe^{4+} or $Fe^{4+}V$ is responsible for this peak, but the fact that it appears only after reduction and can be annealed out by oxidation at moderate temperatures favors the latter. In any case we believe peak No. 1 to be due to an iron impurity level near the valence band.

Peak No. 2 at 0.52 μm (2.4 eV) also seems to be saturable by reduction: This peak is enhanced by Nb doping as one can see by comparing the heights of the peak for the Nb-doped samples in Fig. 4 with

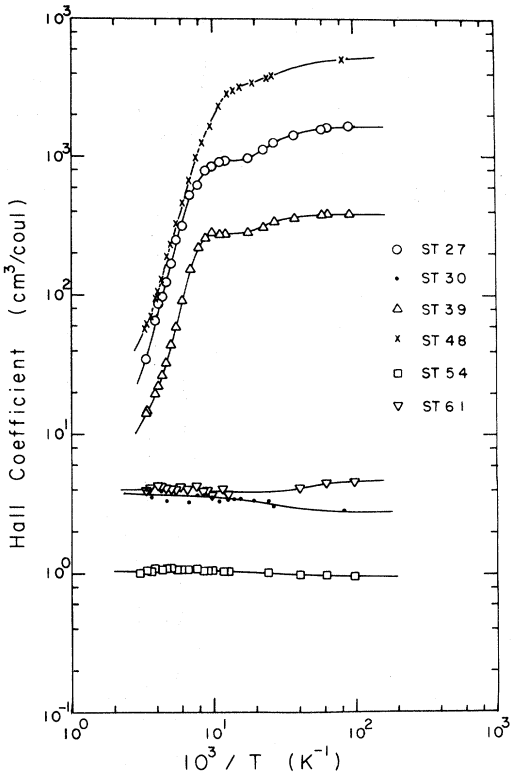

FIG. 11. Log-log plot of Hall coefficient vs reciprocal temperature for various samples.

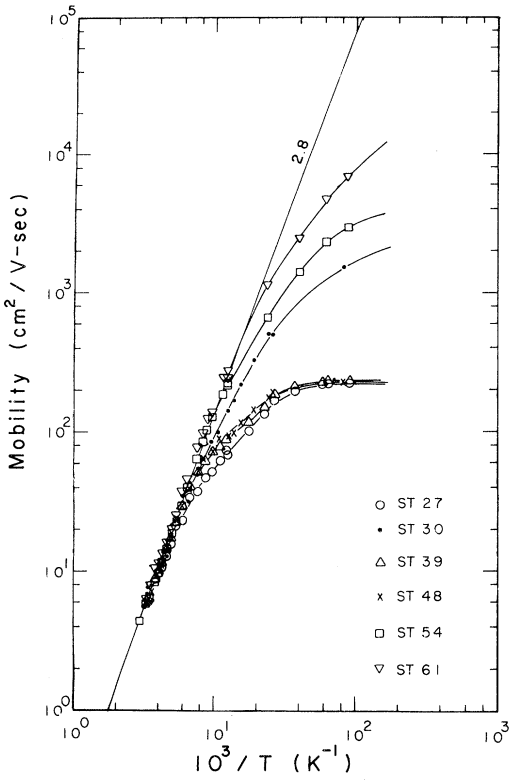

FIG. 12. Log-log plot of Hall mobility vs reciprocal temperature for various samples. The straight line represents the tangent to the mobility curves near room temperature and has slope of 2.8.

those for pure samples in Figs. 1–3. In Fig. 6 typical samples with various sample preparations are compared: Samples 64, 54 and 72 are Nb doped while samples 25 and 30 are undoped. This figure shows clearly that the higher the Nb doping, the stronger becomes the peak. This peak is also easily saturable as can be seen from the oxidation experiment in Figs. 7–9. This peak has a narrow half-width of about 0.2 eV and the carrier concentration is irrelevant to the size of the peak. These facts strongly indicate that it is associated with a Nb impurity.

Yamada *et al.*[10] proposed that both the No. 1 and No. 2 peaks arose from phonon-assisted interconduction-band transitions in line with the interpretation of Simanek *et al.*[30] The results of energy-band calculations,[2,12] however, predict a fairly wide band for interband transitions. In addition, this model would give a nonsaturable peak, contrary to the observed results. Wild *et al.*[11] interpreted the No. 2 peak as being due to a transition from a narrow impurity band formed by oxygen vacancies located 2.4 eV below the bottom of the conduction band. Transport results[3,5] indicate, however, that this level lies rather close to the conduction band, i.e., less than 0.1 eV below the latter. Moreover, this peak seems to saturate easily by reduction, as we have seen earlier, whereas the vacancy concentration would increase indefinitely with increased reduction.[1,3–5,19,31] Furthermore it is absent in several pure, reduced samples (Fig. 2) in agreement with Baer.[9]

We therefore associate this peak with niobium-impurity levels, other than Nb^{5+} ions at titanium sites (which would form very shallow hydrogenic donor levels[1,3,4]). When $SrTiO_3$ is doped with Nb, most Nb atoms go into a Ti site substitutionally to become a Nb^{5+} ion, giving up one electron. Under certain conditions, however, Nb may go into a different site, e.g., interstitial or Sr site, with or without forming a complex with an oxygen vacancy, thus forming a deep, narrow trap. A quick saturation of this peak by reduction and the enhancement of this peak by Nb doping, both of which we have observed, suggest a correlation of this peak with the niobium impurities.

Before discussing the nonsaturable peaks No. 3 and 5, we consider the No. 4 peak which may be caused by defects. This peak appears only in samples which show a carrier freeze-out effect in the Hall measurement: As was mentioned before, the carrier freeze-out effect can be removed by annealing at high temperature before reduction or by Nb doping. Paladino *et al.*[32] and Saifi[33] could reduce the dislocation density considerably by 1800 °C annealing in air, whereas Rhodes and Kingery[34] were able to increase the density by plastic deformation at 1400 °C by a factor 100. This means that dislocations hardly anneal below 1400 °C. Thus we expect a lower dislocation density in our high-temperature annealed crystal (ST30 in Figs. 2 and 3) than in the other nonannealed pure samples. If we compare the absorption curve for ST30 with that for the nonannealed sample ST32 in Fig. 2, which shows about equal absorption, we notice a remarkable difference in the size of No. 4 peak at 1.2 μm between these samples. We found on the other hand that Nb-doped crystals were mechanically more stable and more resistive to thermal shock than nondoped crystals. This indicates that the dislocation density is lower in Nb-doped samples than in pure samples. From the fact that the No. 4 peak is missing or very small for the high-temperature-annealed sample ST30 and all Nb-doped samples (Figs. 1–6), we conclude that dislocations are responsible for this peak, forming deep and wide trap levels in the gap. This peak cannot be easily removed by oxidation as may be expected from the fact that the dislocations hardly anneal out below 1400 °C.[34] In Figs. 7 and 8, we see this clearly. Before oxidation, the No. 3 peak was the larger and the No. 4 peak shows up as a shoulder. After

300 °C oxidation, the No. 4 peak is the major peak with the No. 3 peak showing only as a shoulder (Fig. 8). After 370 °C oxidation, the No. 3 peak is absent and the absorption curve shows clearly a now prominent No. 4 peak (Fig. 7). These observations, are consistent with our model for this peak. The proton-irradiated sample (RST1 in Fig. 2) has a larger shoulder and this is consistent with our assignment of dislocations as being responsible to this peak. We expect of the proton-irradiated sample to have more defects, in particular, more dislocations.

We now turn to a discussion of the nonsaturable peaks, Nos. 3 and 5. The size of the No. 3 peak can be increased indefinitely by reduction but is not necessarily proportional to the carrier concentration. Indeed, Nb-doped samples without any reduction may have a fairly high carrier concentration but show a very small No. 3 peak, if any (Fig. 4; ST62, and ST73). On reduction the No. 3 peak grows indefinitely (Figs. 1–6). Since oxygen vacancies are produced by the reduction process[19,31,32,34,35] this peak must be associated with the vacancy. Transitions between the lower conduction bands at the Γ and X points are forbidden on symmetry grounds.[36] It is possible that the introduction of vacancies relaxes this condition. The Nb impurities substituting on the Ti sites give very shallow hydrogenic levels with negligible effect on the crystal symmetry and would not lead to any absorption. Thus we see the No. 3 peak only in reduced samples.

An alternative explanation for this peak is the following. Since an oxygen vacancy can trap two electrons, the level with only one electron trapped should be much deeper than the level with two electrons. Then the transition from this deep level to the conduction bands gives rise to the No. 3 peak. The upper level (with two electrons) may lie from nearly zero up to 0.1 eV below the conduction band depending on the sample preparation. The lower level may lie much deeper, i.e., 1.7 eV below the conduction band, since the dielectric screening for this tightly bound electron will be drastically reduced as the Bohr radius is reduced. We may also regard this deep level as being analogous to an F center. Then the transition from an s to p state could give rise to a broad peak.

Peak No. 5 near 5 μm (~0.25 eV) is found in all conducting samples for any kind of treatment. The size of the peak grows indefinitely by Nb doping and by reduction, and is roughly proportional to the carrier concentration. These facts underline the nonsaturable nature of this peak as we shall see. According to symmetry arguments, only the $\Delta_{2'} - \Delta_5$ transition along the ⟨100⟩ direction is allowed. In the case of reduced samples with un-ionized vacancy levels, transitions from these vacancy levels to a branch of the conduction band (Δ_5) are also possible. We propose that the No. 5 peak is caused both by the transitions from $\Delta_{2'}$ to Δ_5 and from the shallow occupied vacancy levels to the Δ_5 band. The size of the No. 5 peak should then be a direct measure of the carrier concentration as observed. According to the Mattheiss model,[12] the conduction-band minimum lies at the zone center (Γ point), so that the conduction electrons lie near that point. Therefore the energy of the transition is rather small and varies depending on the carrier concentration. We could not confirm this concentration dependence of the position of this peak due to the difficulty in measuring the absorption for samples with high carrier concentrations. In Kahn and Leyendecker's model,[2] on the other hand, the conduction-band minima lie at the zone edge in the ⟨100⟩ direction (X point) and consequently one would expect a sharp absorption peak centered at 0.6 eV for small carrier concentrations, contrary to the observed results. Thus, the Mattheiss model fits our data better.

Baer[9] observed a gradual falling off of the free-carrier absorption tail starting at 2.5 μm and reaching a saturation at 4 μm, which was the limit of his observations, and therefore did not see the peak. He interpreted this flattening off to be due to the factor, $(1 - \lambda/\lambda_l)^{1/2}$ in the asymptotic expression of Gurevich *et al.* for the absorption coefficient for LO-mode scattering.[16] The exact expression for LO-mode scattering,[16] however, indicates that there should be an absorption peak near $\lambda = \lambda_l$ for $\hbar\omega_l \gtrsim 4kT$. Since $\lambda_l = 12.5$ μm for the first (highest) LO mode, this peak should appear at 12.5 not at 4.8 μm. This suggests that the No. 5 peak is not due to free-carrier absorption.

B. New interpretation of the "free-carrier absorption tails"

Baer[9] observed the wavelength dependence of absorption in his reduced samples to follow a $\lambda^{2.5}$ law in the wavelength range between 0.6 and 2.5 μm. From this he concluded that the absorption was due to the free carriers with LO-mode scattering. However, his results show the bending of the tail to start at about 2.5 μm which he interpreted as due to the $(1 - \lambda/\lambda_l)^{1/2}$ factor in the absorption. As we see in Figs. 1, 2, 4, 5, 7, and 9, the absorption tails between 1 and 2.5 μm are not strictly straight lines on a log-log plot, but their slopes change continuously with wavelength. This, together with the fact that the observed values of the absorption tails are an order of magnitude larger than the theoretical ones, strongly suggests that other mechanisms predominate over the free-carrier scattering. In fact, absorptions involving discrete transitions, combined with free-carrier absorption, lead to a

qualitative fit of our experimental values to the theoretical predictions. It will be remembered that, in our model, the No. 5 peak is due to allowed interconduction-band transitions ($\Delta_{2'} - \Delta_5$), or transitions from filled impurity levels to the empty conduction-band branch. Since these are direct, allowed transitions, their probability of occurrence is much larger than that for free-carrier transitions, which are indirect and phonon assisted. This in itself could explain why the observed value for the absorption is an order of magnitude greater than that calculated. The model implies that the No. 5 peak has a fairly sharp drop, and thus a steep slope, on its short-wavelength end. Thus a superposition of this onto the free-carrier absorption can give a steep slope of more than 3 as observed in the niobium-doped samples (Figs. 4, 5, and 9). Similar arguments obtain for the other samples. In the nonannealed, reduced samples, the existence of the No. 4 peak (at 1.2 μm) together with that of the broad No. 3 peak centered at 0.7 μm makes the slope of the tail less steep than 2.2. As the degree of reduction is decreased in these samples, the size of the No. 4 peak relative to that of the No. 3 peak increases, and the slope of the tail becomes smaller, as is observed (Figs. 1 and 2). In the preannealed sample (ST30), the No. 4 peak is absent, thus giving the steeper slope of 2.6 (Fig. 2).

C. Transport

As stated earlier, electronic transport in semiconducting $SrTiO_3$ can be divided into two types: conduction by free charge carriers in the conduction band, and impurity-band type conduction.[5] As one can see in Figs. 10–12, the conduction in Nb-doped samples (ST61 and ST54) and in a reduced sample preannealed at high temperature (ST30) belongs to the first type and shows no carrier freeze-out effect (Fig. 11). Consequently, the resistivity decreases rapidly as the temperature is lowered owing the decrease in LO-mode scattering. Pure, reduced samples without high-temperature preannealing (ST27, ST39, and ST48), on the other hand, contain the second type and show a carrier freeze-out effect, as seen in Fig. 11, indicating the existence of deep donor levels. This carrier freeze-out effect will not be seen until the levels become deep enough so that they are no longer of a purely hydrogenic type. Tufte and Chapman,[3] in some of their hydrogen-reduced samples (Nos. 3 and 6 in Fig. 2, Ref. 3) observed a rather weak carrier freeze-out effect, implying a small, but non-negligible, ionization energy. The preannealed sample ST30 in Fig. 11 and the samples in the work of Frederikse *et al.*[4] show a decrease in Hall coefficient at low temperature. If the levels are hydrogenic, a relatively deep level with an ionization energy of the order of kT at room temperature (0.025 eV) may not show any carrier freeze-out effect, but rather show a decrease in Hall coefficient at low temperature due to the large increase in dielectric constant at low temperature.[35] On the other hand, some reduced samples (e.g., ST54 in Fig. 11) show a constant Hall coefficient, implying nearly zero ionization energy. Thus vacancy donor levels may be located almost anywhere from nearly zero to about 0.1 eV[5] below the conduction band, depending on sample preparation.

At low temperatures the ionized impurity scattering will dominate over the LO-phonon scattering due to the rapid decrease of the latter. Tufte and Chapman[3] found large discrepancies between observed and calculated values of mobility at low temperature, assuming the carrier concentration to be equal to the ionized impurity concentration. Their calculated value of mobility at 2 K, for a Nb-doped sample, using Mansfield's formula,[17] was 60 times that of the observed value. However, as we saw in our optical absorption experiments, there exist large absorption peaks, which imply the existence of large concentrations of compensating electron-trap levels in the energy gap. The carrier concentration, therefore, is always smaller than the ionized impurity concentration. In fact the carrier concentration in our Nb-doped sample ST61 is only about 30% of the total Nb-impurity concentration assumed to be there. Additional scattering such as by neutral impurities, dislocations, interstitials, and neutral vacancies could reduce the mobility value even further.

In particular, it may be shown that scattering from neutral impurities can be very important for a polar crystal such as $SrTiO_3$. Erginsoy[37] derived the scattering cross section utilizing a result due to Massey and Moiseiwitsch.[38] The mobility is given by:

$$\mu_N = \frac{e}{20\, a_{\mathrm{eff}} \hbar N_N}, \quad E < \tfrac{1}{4} E_i$$

where $a_{\mathrm{eff}} = (\epsilon m/m^*)\, a_0$ is the effective Bohr radius, ϵ the effective dielectric constant, m^*/m the effective—to—free-electron mass ratio, a_0 the first Bohr radius, N_N the concentration of neutral impurities, and E and E_i the electron and the ionization energy of the neutral level, respectively. One sees that, for this type of scattering, the mobility decreases with increases in effective Bohr radius. $SrTiO_3$ has a very large dielectric constant at low temperatures, and thus a large effective Bohr radius. If one takes, as an example, a netural level lying 0.1 eV below the conduction band, as is the case in our unannealed, reduced samples, $a_{\mathrm{eff}} = 10 a_0$ assuming $m^*/m = 2$ and, then, $\mu_N \cong 10^3$ cm^2/V sec compared to $\mu_i \cong 10^5$ cm^2/V sec for the scattering by ionized

impurities in the same concentration, using Mansfield's formula.[17]

V. SUMMARY

A. Optical

(i) There are up to five absorption peaks in semiconducting $SrTiO_3$ throughout the region between the absorption edge and the intrinsic infrared absorption (0.38–7 μm).

(ii) The first (0.43 μm) and second peaks (0.52 μm) are due to the impurities Fe and Nb, respectively.

(iii) The third peak (0.7 μm) is probably due to a transition either from shallow vacancy levels to higher branches of conduction bands or from deep vacancy levels (1.7 eV below the conduction band) to upper excited level (F-center-like).

(iv) The fourth peak (1.2 μm) is due to a trap associated with dislocations.

(v) The fifth peak (~5 μm) is probably due to an interband transition of conduction electrons ($\Delta_{2'} - \Delta_5$) and transitions from shallow donor levels to the Δ_5 conduction band.

(vi) The so-called "free-carrier absorption tail" is not due predominantly to transitions involving free carriers. Instead, it is in large part due to transitions leading to the No. 5 peak, superposed on free-carrier absorption, with additional contributions from peaks No. 4 and 3.

B. Transport

(i) Carrier freeze out in unannealed, reduced crystals can be removed by high-temperature preannealing.

(ii) Nb donor levels are hydrogenic and form very shallow donor levels, whereas vacancy donor levels produced by the reduction process may lie anywhere from nearly zero to 0.1 eV below the bottom of the conduction band depending on the sample preparation.

(iii) The total number of ionized impurities at low temperature is much larger than the carrier concentration due to the existence of large concentrations of compensating trap levels deep in the energy gap.

(iv) Neutral-impurity scattering may be very important at low temperatures for a material with large dielectric constant such as $SrTiO_3$.

ACKNOWLEDGMENTS

The authors are indebted to Professor C. Sandorfy and his colleagues in the Chemistry Department for letting us use some of their experimental facilities. They also wish to thank to Professor D. Matz for helpful discussions. Thanks are also due the members of the Nuclear Physics Laboratory at the University of Montreal for the irradiation work.

---

†Work supported by Le Ministère de l'Education, Province de Québec, and National Research Council of Canada.

*Formerly J. Yahia.

[1] H. P. R. Frederikse, W. R. Thurber, and W. R. Hosler, Phys. Rev. 134, A 442 (1964).
[2] A. H. Kahn and A. J. Leyendecker, Phys. Rev. 135, A 1321 (1964).
[3] O. N. Tufte and P. W. Chapman, Phys. Rev. 155, 796 (1967).
[4] H. P. R. Frederikse and W. R. Hosler, Phys. Rev. 161, 822 (1967).
[5] C. Lee, J. Yahia, and J. L. Brebner, Phys. Rev. B 3, 2525 (1971).
[6] D. Parker and J. Yahia, Phys. Rev. 169, 605 (1968).
[7] H. Yasunaga, J. Phys. Soc. Jpn., 24, 1035 (1968).
[8] H. W. Gandy, Phys. Rev. 113, 795 (1959).
[9] W. S. Baer, Phys. Rev. 144, 734 (1966).
[10] H. Yamada and G. R. Miller, J. Solid State Chem. 6, 169 (1973).
[11] R. L. Wild, E. M. Rockar, and J. C. Smith, Phys. Rev. B 8, 3828 (1973).
[12] L. F. Mattheiss, Phys. Rev. B 6, 4718 (1972).
[13] L. F. Mattheiss, Phys. Rev. B 6, 4740 (1972).
[14] T. Wolfram, E. A. Kraut, and F. J. Morin, Phys. Rev. B 7, 1677 (1973).
[15] S. Visvanathan, Phys. Rev. 120, 376 (1960).
[16] V. L. Gurevich, I. G. Lang, and Yu. A. Firsov, Fiz. Tverd. Tela 4, 1252 (1962) [Sov. Phys.-Solid State 4, 918 (1962)].
[17] R. Mansfield, Proc. Phys. Soc. Lond. B 69, 76 (1956); E. Conwell and V. F. Weisskopf, Phys. Rev. 77, 388 (1950); H. Brooks, Phys. Rev. 83, 879 (1951).
[18] B. W. Faughnan, Phys. Rev. B 4, 3623 (1971).
[19] J. Blanc and D. L. Staebler, Phys. Rev. 134, 3548 (1971).
[20] F. J. Morin and J. R. Oliver, Phys. Rev. B 8, 5847 (1973).
[21] O. N. Tufte and E. L. Stelzer, Phys. Rev. 173, 775 (1968).
[22] H. P. R. Frederikse, W. R. Hosler, and W. R. Thurber, J. Phys. Soc. Jpn. Suppl. 21, 32 (1966).
[23] A. S. Barker, in *Proceedings of the International Colloquium on Optical Properties and Electronic Structure of Metals and Alloys, Paris* 1965 (North-Holland, Amsterdam, 1966).
[24] M. J. G. Meyer, Phys. Rev. 112, 298 (1958).
[25] R. Rosenberg and M. Lax, Phys. Rev. 112, 843 (1958).
[26] S. Visvanathan, Phys. Rev. 120, 379 (1960).
[27] R. Wolfe, Proc. Phys. Soc. Lond. A 67, 74 (1954).
[28] H. Y. Fan, Rep. Prog. Phys. 14, 107 (1956).
[29] B. W. Faughnan and Z. J. Kiss, Phys. Rev. Lett. 21, 1331 (1968).
[30] E. Simanek, N. L. Huang-Liu, and R. L. Wild, J. Phys. Chem. Solids 33, 951 (1971).
[31] A. E. Paladino, J. Am. Ceram. Soc. 48, 476 (1965).
[32] A. E. Paladino, L. G. Rubin, and J. S. Waugh, J. Phys. Chem. Solids 26, 391 (1965).
[33] M. A. Saifi, Ph. D. thesis (Pennsylvania State University, 1968) (unpublished).

[34]W. H. Rhodes and W. D. Kingery, J. Am. Ceram. Soc. 49, 521 (1966).
[35]L. C. Walters and R. E. Grace, J. Phys. Chem. Solids 28, 245 (1967).
[36]See, for example, D. L. Greenaway and G. Harbeke, *Optical Properties and Structure of Semiconductors* (Pergamon, London, 1968), and references given therein.
[37]C. Erginsoy, Phys. Rev. 79, 1013 (1950).
[38]H. S. W. Massey and B. L. Moiseiwitsch, Phys. Rev. 78, 180 (1950).